

Geometric Origin of the Tennis Racket Effect

P. Mardešić*, L. Van Damme, G. J. Gutierrez Guillen, D. Sugny†

March 31, 2020

Abstract

The tennis racket effect is a geometric phenomenon which occurs in a free rotation of a three-dimensional rigid body. In a complex phase space, we show that this effect originates from a pole of a Riemann surface and can be viewed as a result of the Picard-Lefschetz formula. We prove that a perfect twist of the racket is achieved in the limit of an ideal asymmetric object. We give upper and lower bounds to the twist defect for any rigid body, which reveals the robustness of the effect. A similar study allows us to explore in which conditions the Monster flip, an almost impossible skate board trick, can be realized.

Consider an experiment that every tennis player has already made. The tennis racket is held by the handle and thrown in the air so that the handle makes a full turn before catching it. Assume that the two faces of the head can be distinguished. It is then observed, once the racket is caught, that the two faces have been exchanged. This means that the racket did not perform a simple rotation around its axis, but also an extra half-turn. This twist, which is schematically represented in Fig. 1, is called the tennis racket effect (TRE). It is also known as Djanibekov effect, named after the Russian astronaut who made it in 1985 with a wing nut in zero gravity. The Monster Flip Effect (MFE) is a free style skate board trick which can only be realized by expert skate boarders. It consists in jumping with the skateboard and making it turn around its transverse axis with the wheels falling back to the ground. This trick is very difficult to execute since TRE predicts precisely the opposite, turning about this axis should produce a π - flip and the wheels should end up in the air. The video [1] shows that this trick can be made with success after several attempts.

How to explain and describe these two phenomena? A first approach consists in modeling these two motions as a free rotation of an asymmetric rigid body, which has three different moments of inertia along its three inertia axes [2]. The axes with the smallest and largest moments of inertia are stable, while the intermediate one is unstable. It is precisely this instability which is at the origin of TRE [3]. A more detailed description can be obtained from the Euler equations which govern the free rotational dynamics of a rigid body. This

*Institut de Mathématiques de Bourgogne - UMR 5584 CNRS, Université de Bourgogne-Franche Comté, 9 avenue Alain Savary, BP 47870, 21078 DIJON, France, pavao.mardesic@u-bourgogne.fr

†Laboratoire Interdisciplinaire Carnot de Bourgogne (ICB), UMR 6303 CNRS-Université Bourgogne-Franche Comté, 9 Av. A. Savary, BP 47 870, F-21078 Dijon Cedex, France, dominique.sugny@u-bourgogne.fr

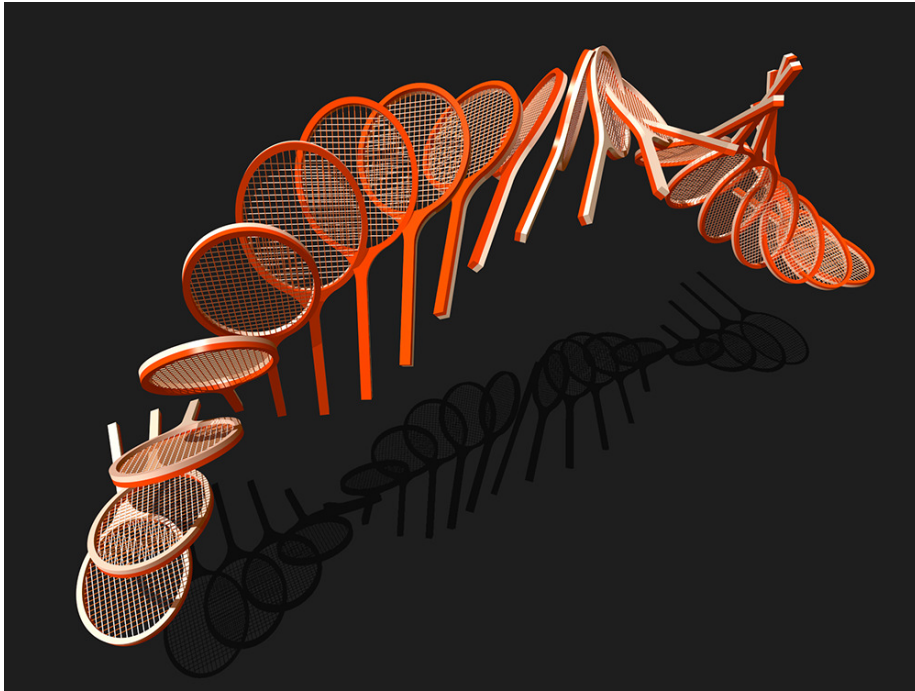


Figure 1: (Color online) Illustration of the Tennis Racket Effect: The head of the racket performs a π - flip when the handle makes a 2π - rotation.

three-dimensional rotation is an example of Hamiltonian integrable systems [4] in which the system trajectories can be expressed analytically. The dynamics of the rigid body in the space-fixed frame are given by elliptic integrals of the first and third kinds, which lead to a very accurate description of TRE [3, 5, 6]. However, this analysis does not reveal its geometric character. A geometric point of view provides valuable physical insights, in particular with respect to the robustness of the corresponding physical phenomenon, and is generally the starting point for generalizing the effect under study. In the last decades, different geometric structures have been studied in the context of mechanical systems with a small number of degrees of freedom. Among others, we can mention the Berry phase [7], Hamiltonian monodromy [8, 10, 9], singular tori [11] and the Chern number [12] which found applications in classical and quantum physics. In this letter, we show that the geometric origin of TRE is a pole of a Riemann surface defined in a complex phase space. The robustness of TRE can be deduced from this geometric analysis. From a more fundamental point of view, this effect can be interpreted as the result of the Picard-Lefschetz formula which describes the possible deformation of an integration contour in a complex space after pushing it around a singular fiber [13, 14]. The geometric character of MFE can also be deduced from this approach and helps understanding in which conditions this almost impossible skate board trick can be realized. Similar complex approaches have been used to describe Hamiltonian monodromy [15, 16, 17].

The position of the body-fixed frame (x, y, z) with respect to the space-fixed

frame (X, Y, Z) defines the free rotation of a rigid body [4, 2]. Three Euler angles (θ, ϕ, ψ) characterize the relative motion of the body-fixed frame as shown in Fig. 2. The angle θ is the angle between the axis z and the space-fixed axis Z .

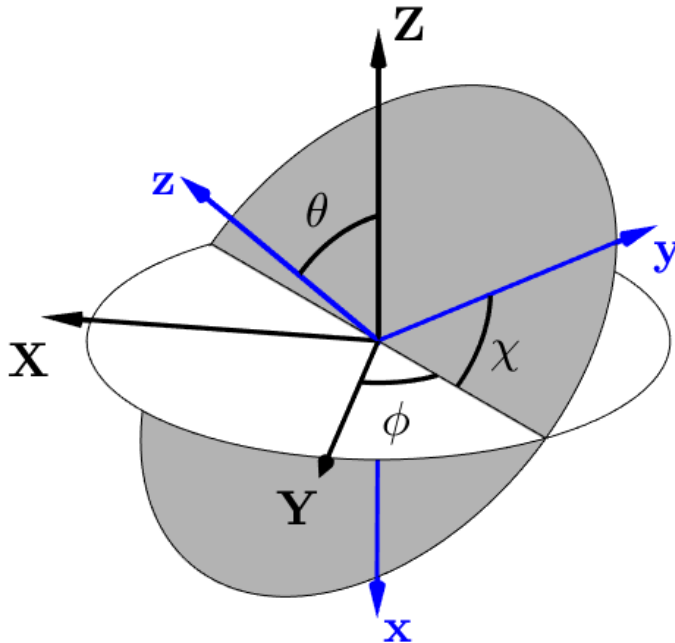


Figure 2: (Color online) Definition of the Euler angles used to describe the position of the body-fixed frame (x, y, z) with respect to the space-fixed frame (X, Y, Z) (see the text for details).

The rotation of the body about the axes Z and z is respectively described by the angles ϕ and ψ . The moments of inertia I_x , I_y and I_z are the elements of the diagonal inertia matrix in the body-fixed frame. We adopt the convention $I_z < I_y < I_x$ for the moments of any asymmetric top. A tennis racket is a standard example of an asymmetric rigid body in which the z -axis is along the handle of the racket, y lies in the plane of the head of the racket and x is orthogonal to the head. A TRE consists in a 2π -rotation of the body around the y -axis. The precession of the handle is measured by the angle ψ . The TRE manifests by a twist of the head of the racket, i.e. by a variation $\Delta\psi = \pi$, along a trajectory such that $\Delta\phi = 2\pi$ [6].

Rotational motion is described by integrable dynamics which have two constants of the motion, namely the angular momentum \mathbf{J} and the Hamiltonian H . The Z -axis of the space-fixed frame is usually chosen along the direction of \mathbf{J} . In the body-fixed frame, the components of \mathbf{J} can be expressed as

$J_x = -J \sin \theta \cos \psi$, $J_y = J \sin \theta \sin \psi$ and $J_z = J \cos \theta$, where J is the modulus of \mathbf{J} , while H is given by $H = \frac{J_x^2}{2I_x} + \frac{J_y^2}{2I_y} + \frac{J_z^2}{2I_z}$. In the (J_x, J_y, J_z) -space, the energy of the intermediate axis $\frac{J^2}{2I_y}$ defines the position of the separatrix which connects the unstable fixed points and is also the boundary between the rotating and oscillating trajectories for $2I_y H > J^2$ and $2I_y H < J^2$, respectively. Using the angular velocities $\Omega_k = J_k/I_k$, $k = x, y, z$, it follows that the Euler angles satisfy the Euler differential system:

$$\begin{aligned}\dot{\theta} &= J \left(\frac{1}{I_y} - \frac{1}{I_x} \right) \sin \theta \sin \psi \cos \psi \\ \dot{\phi} &= J \left(\frac{\sin^2 \psi}{I_y} + \frac{\cos^2 \psi}{I_x} \right) \\ \dot{\psi} &= J \left(\frac{1}{I_z} - \frac{\sin^2 \psi}{I_y} - \frac{\cos^2 \psi}{I_x} \right) \cos \theta\end{aligned}\tag{1}$$

We introduce the parameters $a = \frac{I_y}{I_z} - 1$, $b = 1 - \frac{I_y}{I_x}$ and $c = \frac{2I_y H}{J^2} - 1$, with the constraint $-b < c < a$. Note that c measures the signed distance to the separatrix. The parameters a and b , with $a > 0$ and $0 < b < 1$, give information about the asymmetry of the rigid body. The cases $a = 0$ and $b = 0$ are associated to a symmetric top. In the limit of a perfect asymmetric body, $I_z \ll I_y \ll I_x$, we deduce that $b \rightarrow 1$ and $a \rightarrow +\infty$. For a standard tennis racket, we have $a = 12.53$ and $b = 0.063$ [18] while for a skate board the parameters are $a = 8.82$ and $b = 0.078$ (see Sup. Sec. I).

TRE is a geometric phenomenon which does not depend on time. Using Eq. (1), it can be described by the evolution of ψ with respect to ϕ :

$$\frac{d\psi}{d\phi} = \frac{(a + b \cos^2 \psi) \cos \theta}{1 - b \cos^2 \psi}.\tag{2}$$

From $c = a - \sin^2 \theta (a + b \cos^2 \psi)$, we arrive at:

$$\cos \theta = \pm \sqrt{\frac{c + b \cos^2 \psi}{a + b \cos^2 \psi}},\tag{3}$$

which leads to:

$$\frac{d\psi}{d\phi} = \pm \frac{\sqrt{(a + b \cos^2 \psi)(c + b \cos^2 \psi)}}{1 - b \cos^2 \psi}.\tag{4}$$

In the rest of the paper, we consider only the positive values of $\frac{d\psi}{d\phi}$, the same analysis can be done for the negative sign. We will extend below the study to the complex domain and continue analytically all the functions. Equation (16) can be used to define a two-dimensional reduced phase space with respect to ψ and $d\psi/d\phi$, as displayed in Fig. 3. Note the similarity of this phase space with the one of a planar pendulum, except that two consecutive unstable fixed points are separated by π instead of 2π .

TRE is associated with a trajectory for which $\Delta\psi \simeq \pi$ when $\Delta\phi = 2\pi$. We denote by ψ_0 and ψ_f the initial and final values of the angle ψ . To simplify the study of TRE, we consider a symmetric configuration for which $\psi_0 = -\frac{\pi}{2} + \epsilon$ and $\psi_f = \frac{\pi}{2} - \epsilon$. A perfect TRE is thus achieved in the limit $\epsilon \rightarrow 0$. Note

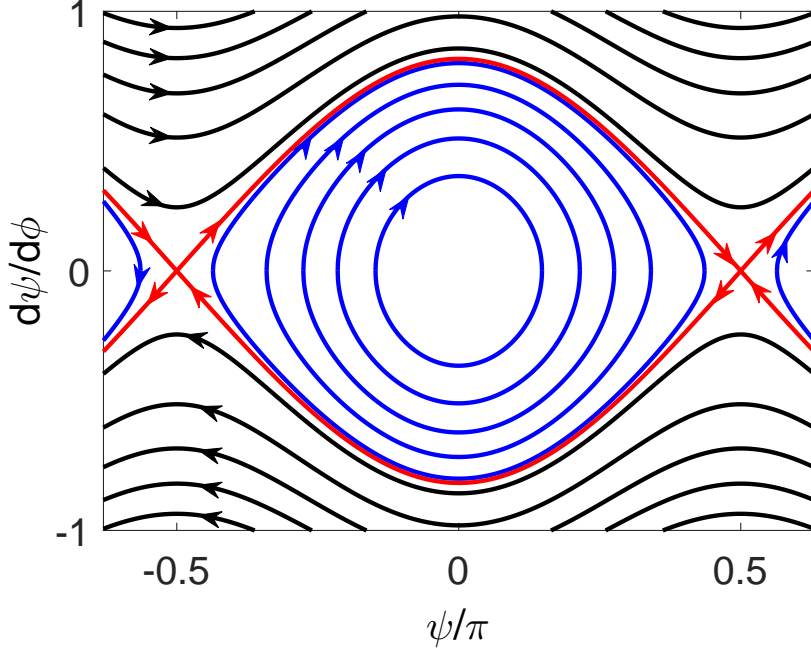


Figure 3: (Color online) Reduced phase space describing the dynamics of the rigid body in the space $(\psi, d\psi/d\phi)$. The black and blue (dark gray) lines depict respectively the rotating and oscillating trajectories of the angular momentum. The solid red line (light gray) represents the separatrix. The parameters a and b are set respectively to 12 and 0.05.

that this symmetry hypothesis is not restrictive as shown numerically in Sup. Sec. IV. Using Eq. (16), we obtain that the variation of ϕ is given by:

$$\Delta\phi = \int_{-\frac{\pi}{2}+\epsilon}^{\frac{\pi}{2}-\epsilon} \frac{1 - b \cos^2 \psi}{\sqrt{(a + b \cos^2 \psi)(c + b \cos^2 \psi)}} d\psi. \quad (5)$$

For oscillating trajectories, the condition $c + b \cos^2 \psi \geq 0$ leads to $\sin^2 \epsilon \geq |\frac{c}{b}|$. From the parity of the integral and the change of variables $x = \cos^2 \psi$, $\Delta\phi$ can be expressed as an incomplete elliptic integral:

$$\Delta\phi(\epsilon) = \int_{\sin^2 \epsilon}^1 \omega, \quad (6)$$

with

$$\omega = \frac{1}{b} \frac{1 - bx}{\sqrt{x(x - \beta)(1 - x)(x - \alpha)}} dx, \quad (7)$$

where $\alpha = -\frac{a}{b}$ and $\beta = -\frac{c}{b}$. As explained in Sup. Sec. II, we introduce a function M defined by $M(u_0) = \frac{2 \ln(1+\sqrt{2})}{\sqrt{1-u_0}} + 2 \ln(2)$ for $u_0 \in]0, 1[$, and $m = M(\frac{1}{2}) \simeq 3.879$. A precise description of TRE is given by Theorem 1, which is the main result of this study.

Theorem 1. For all c such that:

$$|c| < b \exp(-2\pi\sqrt{ab} - m),$$

for ab large enough, the equation

$$\Delta\phi_{a,b,c}(\epsilon) = 2\pi$$

has a unique solution $\epsilon_S(a, b, c)$ which verifies:

$$\arcsin\left[\sqrt{\left|\frac{c}{b}\right|}\right] < \epsilon_S < \arcsin\left[\exp(-\pi\sqrt{ab} - \frac{m}{2})\right]. \quad (8)$$

This leads to:

$$\lim_{ab \rightarrow +\infty} \epsilon_S(a, b, c) = 0.$$

A few comments are in order here. For a sufficiently asymmetric body with $ab \gg 1$, Theorem 1 states the existence and uniqueness of a symmetric configuration realizing the TRE. The corresponding trajectory is closer and closer to the separatrix for more asymmetric body (i.e. c goes to 0). Theorem 1 also establishes the robustness of the effect with respect to the shape of the body. The twist of the head is exactly π in the limit of a perfect asymmetric object. Lower and upper bounds to the twist defect are given by Eq. (8) as a function of the different parameters. The statement is true slightly more generally for any value $u_0 \in]0, 1[$, by replacing everywhere $m = M(1/2)$ by $M(u_0)$. We put in Theorem 1 $u_0 = 1/2$ for simplicity. These results have a geometric origin described below.

We study the solution ϵ of $\Delta\phi_{a,b,c}(\epsilon) = 2\pi$, where $\Delta\phi = \Delta\phi_{a,b,c}$ is given by Eq. (5). The origin of TRE is revealed by a complexification of the problem in which $\Delta\phi$ can be interpreted as an Abelian integral over the Riemann surface of the form ω [14]. As displayed in Fig. 4, this surface has two sheets with four branch points in $x = 0, 1, \beta$ and α . Branch cuts are introduced to define a single-valued function. In the limit $c \rightarrow 0$, the two branch points $x = 0$ and $x = \beta$ coincide, leading to a pole whose integral is the logarithmic function. Since we consider large values of a , note that there is no confluence of the branch point $x = \alpha$ with $x = \beta$ or 0.

Let F be the function defined by:

$$F_{a,b,c}(u) = \int_u^1 \omega = \int_\gamma \omega,$$

where γ is the integration path with $0 < u < 1$. We have $\Delta\phi_{a,b,c}(\epsilon) = F_{a,b,c}(\sin^2 \epsilon)$. The multi-valued character of $F_{a,b,c}$ is different for $u < |\beta|$ and $u > |\beta|$. Note that the first case only concerns the rotating trajectories with $c > 0$. In the case $|\beta| < u < 1$, we consider in the upper sheet of the Riemann surface the cycle δ passing by $x = u$ and encircling the two branch points β and 0, as displayed in Fig. 4. By the Picard-Lefschetz formula [13, 14], the integration contour γ is deformed to itself plus δ when the point $x = u$ performs a loop along δ . The integral $\int_\delta \omega$ adds to $F_{a,b,c}$, which reveals the multi-valued character of $F_{a,b,c}$ as a complex function. A single-valued function can be obtained by adding a convenient multiple of $\ln u = -\int_u^1 \frac{dx}{x}$, the factor being given

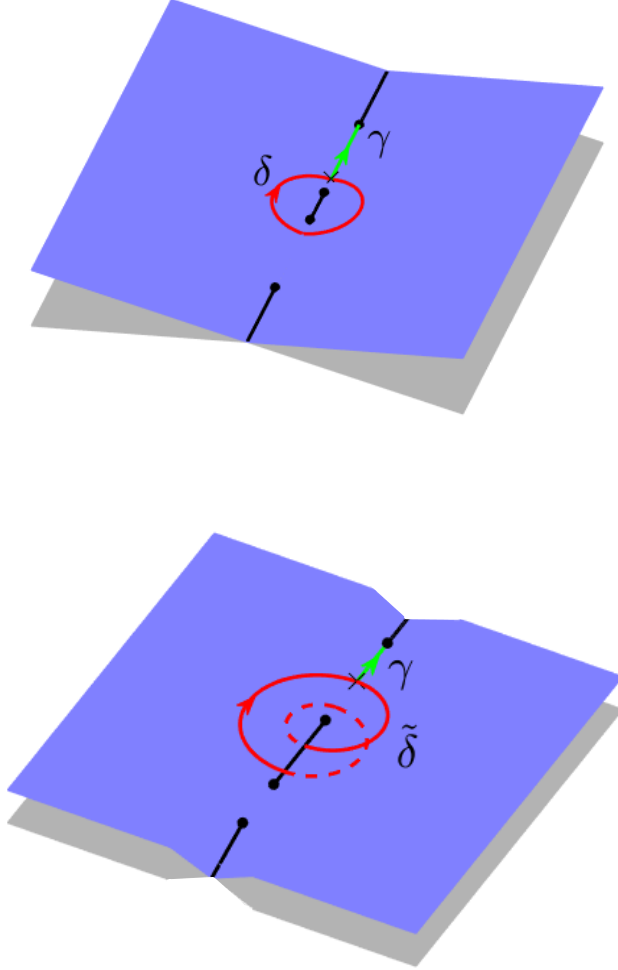


Figure 4: (Color online) Riemann surface of the form ω with the four branch points (black dots) in $x = \alpha$, $x = \beta$, $x = 0$ and $x = 1$ (from bottom to top). When $c \rightarrow 0$, the two points $x = \beta$ and $x = 0$ coincide and give birth to a pole. The top and bottom panels represent the cases where the TRE can or cannot be observed. The solid straight lines represent the branch cuts of the surface. The cycles δ and $\tilde{\delta}$ are depicted by solid red (dark gray) lines. The form ω is integrated along the path γ between the point u (black cross) and the ramification point $x = 1$ (green or light gray solid line).

by $\frac{1}{2\pi i} \int_{\delta} \omega$. In the limit $c \rightarrow 0$, ω has a pole in $x = 0$ and this integral can be computed from a residue formula.

We present a heuristic proof of Theorem 1, while a rigorous demonstration is provided in Sup. Sec. II. We consider a simplified version of the problem where

only two branch points are accounted for. We have:

$$\int_u^1 \frac{1}{\sqrt{x(x-\beta)}} dx = 2 \ln(\sqrt{x-\beta} + \sqrt{x}) \Big|_{x=u}^1.$$

Using the pole at infinity, we deduce that $\frac{1}{2\pi i} \int_{\delta} \frac{dx}{x} = 1$ and:

$$\int_u^1 \left[\frac{1}{\sqrt{x(x-\beta)}} - \frac{1}{x} \right] dx = 2 \ln \left(\frac{1 + \sqrt{1-\beta}}{1 + \sqrt{1-\frac{\beta}{u}}} \right),$$

which is a well-defined and bounded function of u for $|\beta| < u < 1$. As shown in Sup. Sec. II, this argument can be generalized to $F_{a,b,c}$ which can be expressed as:

$$F_{a,b,c}(u) = \frac{1}{\sqrt{ab}} h_{a,b,c}(u) - \frac{1}{\sqrt{ab}} \ln u, \quad (9)$$

where $h_{a,b,c}$ is an analytic and bounded function in $]|\beta|, u_0[$ with $0 < u_0 < 1$. The bound of $h_{a,b,c}$ is the function M introduced in Theorem 1 and derived in Sup. Sec. II. For ab large enough, it is then straightforward to show that the equation $F_{a,b,c}(u) = 2\pi$ has a unique solution and to prove Theorem 1. In the second region in which $u < |\beta|$, the geometric situation is completely different as can be seen in Fig. 4. The cycle $\tilde{\delta}$ encircles only the branch point $x = 0$ and no pole occurs when $c \rightarrow 0$. Turning twice around $x = 0$ to get a closed path, we obtain $\int_{\tilde{\delta}} \omega = 0$. This result stems from integrating the complex function $x \mapsto \frac{1}{\sqrt{x}}$ along $\tilde{\delta}$. We therefore deduce that the function $F_{a,b,c}$ is bounded with no logarithmic divergence. No information is gained about the existence, the uniqueness and the value of ϵ , i.e. the possibility to realize TRE.

The Monster Flip, a skate board trick, can be analyzed along the same lines. For this rigid body, the z - and y - inertia axes are respectively orthogonal and parallel to the wheel axis, while the x - axis is orthogonal to the board. As mentioned above, the skate board has to realize a complete turn around its transverse axis together with a small variation of the angle ψ . This motion can be realized in a neighborhood of the unstable point where $\frac{d\psi}{d\phi} = 0$ (i.e. $\frac{d\phi}{d\psi} = \infty$). We search for a solution ϵ close to zero of the equation $\tilde{\Delta}\phi(\epsilon) = 2\pi$ where

$$\tilde{\Delta}\phi(\epsilon) = 2 \int_{\psi_i}^{\frac{\pi}{2} + \epsilon} \frac{1 - b \cos^2 \psi}{\sqrt{a + b \cos^2 \psi} \sqrt{c + b \cos^2 \psi}} d\psi, \quad (10)$$

with $\psi_i = \pi/2$ and $\psi_i = \pi/2 + \arcsin[\sqrt{|\beta|}]$ for rotating and oscillating trajectories, respectively. With the same change of variables as in TRE and for the same form ω defined by Eq. (7), we get:

$$\tilde{\Delta}\phi(\epsilon) = \int_{\cos^2 \psi_i}^{\sin^2 \epsilon} \omega.$$

Introducing $\tilde{F}_{a,b,c}(u) = \int_{\cos^2 \psi_i}^u \omega$, it can be shown in the region $|\beta| < u < 1$ that (see Sup. Sec. III):

$$\tilde{F}_{a,b,c}(u) = \frac{1}{\sqrt{ab}} \tilde{h}_{a,b,c}(u) + \frac{1}{\sqrt{ab}} \ln(u),$$

where $\tilde{h}_{a,b,c}$ is a bounded and single-valued function. Note the change of sign in front of the logarithmic term in the above expression with respect to Eq. (9), which is due to the fact that u appears in the upper bound of integration, whereas it is in the lower bound in TRE. The solution of $\Delta\phi_{a,b,c} = \tilde{F}_{a,b,c}(u)$ can be approximated as:

$$\epsilon \simeq \frac{\sqrt{|\beta|}}{2} e^{\pi\sqrt{ab}}. \quad (11)$$

The accuracy of this approximation is shown numerically in Sup. Sec. IV. For an asymmetric body with $ab \geq 1$, we deduce that the MFE can be observed only in a neighborhood of the separatrix where $|\beta| \ll 1$. The rotation of the skateboard around its transverse axis is, in addition, constrained by the condition $\epsilon \geq \sqrt{|\beta|}$. This result quantifies the difficulty of performing the MFE. For an angle ϵ of 30 degrees, this leads for a standard skate board to $c \simeq 10^{-3}$, while the maximum value of c is of the order of 10. However, note that there are two aspects which help performing MF in practice and which have been neglected in this study [1]. The initial movement of the skateboard is not free and a $\pi/2$ -rotation in ϕ with no variation in ψ is essentially realized while two wheels are on the ground. We also think that the gyroscopic effect of the wheels helps realizing this skateboard trick. The modeling of such effects goes beyond the scope of this paper. Finally, as illustrated in Sup. Sec. III, MFE cannot be realized in the second region $u < |\beta|$ for standard asymmetric rigid bodies.

In summary, we have shown that TRE originates from a pole of a Riemann surface and a perfect twist of the head of the racket occurs in the limit of an ideal asymmetric body. Different properties such as the robustness of the effect have been derived from this geometric analysis. As a byproduct, we have established why the MFE is so difficult to perform with a skateboard. We point out that the proof of this paper can be extended to any variation of the angle ϕ such as, e.g., 4π , for which the handle of the racket makes two full turns with a π -flip of the head. The results of this study pave also the way for the analysis of other classical integrable systems and strongly suggest the importance of complex geometry beyond the cases studied in this paper. A possible future direction is the generalization of this study to $SO(n)$, with $n > 3$, for instance in the integrable case of the Manakov top, in which higher dimensional TRE could be defined [19]. Another intriguing question is to transpose this effect to the quantum world. Different molecular systems could show traces of this effect at the quantum scale [20]. An example is given by asymmetric top molecules, such as the water molecule, which are the microscopic equivalent of asymmetric rigid bodies [21]. Another field of applications is the control of quantum systems by external electromagnetic fields [22] using, e.g., the analogy between Bloch and Euler equations [23].

Acknowledgment

We thank S. J. Glaser for many helpful discussions and for providing us Figure 1. This work was supported by the EUR-EIPHI Graduate School (Grant No. 17-EURE-0002)

References

- [1] MONSTER FLIP Trick Challenge, <https://www.youtube.com/watch?v=vkMmbWYnBHg>; Physics girl, *Why this skateboarding trick should be IMPOSSIBLE ft.*

- Rodney Mullen, <https://www.youtube.com/watch?v=yFRPhi0jhGc>
- [2] H. Goldstein, *Classical Mechanics* (Addison-Wesley, Reading, MA, 1950).
 - [3] R. H. Cushman and L. Bates, *Global Aspects of Classical Integrable Systems* (Birkhauser, Basel, 1997).
 - [4] V. I. Arnold, *Mathematical Methods of Classical Mechanics* (Springer-Verlag, New York, 1989).
 - [5] M. S. Ashbaugh, C. C. Chicone and R. H. Cushman, *J. Dyn. Diff. Eq.* **3**, 67 (1991).
 - [6] L. Van Damme, P. Mardešić and D. Sugny, *Physica D* **338**, 17 (2017)
 - [7] A. Bohm, A. Mostafazadeh, H. Koizumi, Q. Niu, and J. Zwanziger, *The Geometric Phase in Quantum Systems* (Springer, Berlin, 2003).
 - [8] K. Efsthathiou, *Metamorphoses of Hamiltonian Systems with Symmetry*, Lecture Notes in Mathematics Vol. 1864 (Springer-Verlag, Heidelberg, 2004)
 - [9] N. J. Fitch, C. A. Weidner, L. P. Parazzoli, H. R. Dullin, and H. J. Lewandowski, *Phys. Rev. Lett.* **103**, 034301 (2009)
 - [10] R. H. Cushman, H. R. Dullin, A. Giacobbe, D. D. Holm, M. Joyeux, P. Lynch, D. A. Sadovskii, and B. I. Zhilinskiĭ, *Phys. Rev. Lett.* **93**, 024302 (2004)
 - [11] D. Sugny, A. Picozzi, S. Lagrange, and H. R. Jauslin, *Phys. Rev. Lett.* **103**, 034102 (2009).
 - [12] F. Faure and B. Zhilinskii, *Phys. Rev. Lett.* **85**, 960 (2000).
 - [13] V. I. Arnol'd, S. M. Goussein-Zade, and A. N. Varchenko, *Singularities of Differentiable Mappings* (Birkhauser, Boston, 1988).
 - [14] H. Zoladek, *The Monodromy Group* (Birkhauser, Boston, 2006).
 - [15] M. Audin, *Commun. Math. Phys.* **229**, 459 (2002).
 - [16] F. Beukers and R. H. Cushman, *Contemp. Math.* **292**, 47 (2002).
 - [17] D. Sugny, P. Mardešić, M. Pelletier, A. Jebrane, and H. R. Jauslin, *J. Math. Phys.* **49**, 042701 (2008).
 - [18] H. Brody, *Phys. Teach.* 213 (1985)
 - [19] A. M. Perelomov, *J. Phys. A* **38**, 801 (2005).
 - [20] C. P. Koch, M. Lemeshko and D. Sugny, *Rev. Mod. Phys.* **91**, 035005 (2019)
 - [21] K. Hamraoui, L. Van Damme, P. Mardesic and D. Sugny, *Phys. Rev. A* **97**, 032118 (2018)
 - [22] S. J. Glaser, U. Boscain, T. Calarco, C. P. Koch, W. Köckenberger, R. Kosloff, I. Kuprov, B. Luy, S. Schirmer, T. Schulte-Herbrüggen, D. Sugny, and F. K. Wilhelm, *Eur. Phys. J. D* **69**, 279 (2015)

- [23] L. Van Damme, D. Leiner, P. Mardesić, S. J. Glaser and D. Sugny, Sci. Rep. **7**, 3998 (2017)

Supplemental material: Geometric Origin of the Tennis Racket Effect

1 The model system

This paragraph gives some details about the different model systems used in this paper. We recall, in particular, how the moments of inertia can be estimated for different rigid bodies.

The direction of the inertia axes of a standard tennis racket is represented in Fig. 5.

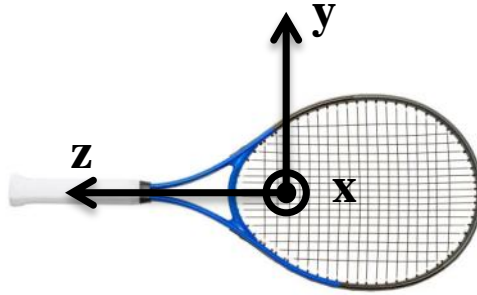


Figure 5: (Color online) A tennis racket with the definition of the inertia axes (x , y , z).

The Tennis Racket Effect can be observed with a book or a mobile phone. If the object of mass m is a homogeneous rectangular cuboid of height h , length L and width l , with $h < l < L$ then the moments of inertia are given by:

$$\begin{cases} I_x = \frac{m}{12}(L^2 + l^2) \\ I_y = \frac{m}{12}(L^2 + h^2) \\ I_z = \frac{m}{12}(h^2 + l^2) \end{cases}$$

We deduce that:

$$a = \frac{L^2 - l^2}{h^2 + l^2}$$
$$b = \frac{l^2 - h^2}{L^2 + l^2}$$

If the object is almost flat, the height will be very small with respect to the other dimensions. In this case, the intermediate axis is in the plane of the object and

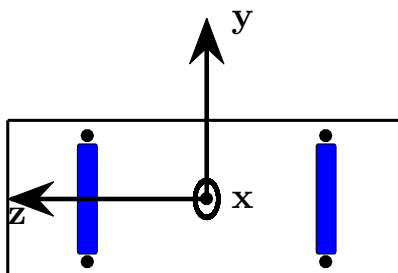


Figure 6: (Color online) Schematic representation at the scale of a skate board with the definition of the inertia axes (x, y, z) . The big dots indicate the position of the wheels and the blue rectangles the trucks.

Table 1: Numerical values of the parameters a and b for different objects. The book is the book of mechanics by Goldstein. The mobile phone is a Samsung JS.

Object	a	b	ab
Racket	12.54	0.06	0.75
Book	1.11	0.31	0.34
Mobile phone	2.97	0.198	0.59
Skate board	8.82	0.078	0.69

perpendicular to the largest side. Numerical values are given in Tab. 1. The computation is more involved for a skate board since the wheels and the truck have to be accounted for. We consider the mass repartition given in Fig. 6 of a skate of length $L = 80$ cm, width $l = 20$ cm and height $h = 5$ cm. The masses of the board, a wheel and a truck are estimated to be respectively of the order of 500 g, 200 g and 350 g, which leads to a total mass of 2 kg. We obtain $I_x = 0.123$ kg m², $I_y = 0.113$ kg m² and $I_z = 0.012$ kg m².

2 Geometric proof of the Tennis Racket Effect

We show rigorously in this section the different statements about the Tennis Racket Effect.

2.1 Analysis of the region $|\beta| < |u| < 1$

We study in this paragraph the function $F_{a,b,c}$ defined in Eq. (9) of the main text. From the geometric analysis in the complex space, the Picard-Lefschetz formula states that the function $F_{a,b,c}$ can be expressed in the complex domain

$\mathcal{A} = \{u \in \mathbb{C} : |\beta| < |u| < 1\}$ as:

$$F_{a,b,c}(u) = g_{a,b,c}(u) - k_{a,b,c}(u) \ln u,$$

where g and k are two holomorphic functions on the annulus \mathcal{A} , which are uniformly bounded and continuous on the closed annulus $\bar{\mathcal{A}}$. Note that $k_{a,b,c}$, which is given by $\frac{1}{2\pi i} \int_{\delta} \omega$, can be determined in the limit $c \rightarrow 0$ from a residue computation. However, in this example, a better upper bound and a precise expression can be derived respectively for $g_{a,b,c}$ and $k_{a,b,c}$ by considering real integrals.

Analysis of $F_{a,b,c}$ in the real case:

The function $F_{a,b,c}$ can be expressed as:

$$F_{a,b,c}(u) = \frac{1}{\sqrt{ab}}(h_1(u) + h_2(u)) - \frac{\ln(u)}{\sqrt{ab}},$$

with

$$h_1(u) = \int_u^1 \left(\frac{1}{\sqrt{x(x-\beta)}} - \frac{1}{x} \right) \frac{1-bx}{\sqrt{(1-x)(1-\frac{x}{\alpha})}} dx,$$

and

$$h_2(u) = \int_u^1 \frac{dx}{x} \left[\frac{1-bx}{\sqrt{(1-x)(1-x/\alpha)}} - 1 \right].$$

We first determine a bound in the real domain of the h_1 -function. Let $0 < u_0 < 1$ such that $0 \leq |\beta| < u \leq u_0 < 1$. Since

$$\frac{1-bx}{\sqrt{(1-x)(1+xa/b)}} \leq \frac{1}{\sqrt{1-u_0}},$$

for $x \in]0, u_0]$, we deduce that:

$$|h_1(u)| \leq \frac{1}{\sqrt{1-u_0}} \int_u^1 \left| \frac{1}{\sqrt{x(x-\beta)}} - \frac{1}{x} \right| dx.$$

which gives

$$|h_1(u)| \leq \frac{1}{\sqrt{1-u_0}} \left| \int_u^1 \left(\frac{1}{\sqrt{x(x-\beta)}} - \frac{1}{x} \right) dx \right|.$$

because the sign of the integrand does not change in $]|\beta|, u_0]$. As in the simplified case of the main text, we use the fact that:

$$\int_u^1 \left(\frac{1}{\sqrt{x(x-\beta)}} - \frac{1}{x} \right) dx = 2 \ln \left(\frac{1 + \sqrt{1-\beta}}{1 + \sqrt{1-\beta/u}} \right),$$

and we arrive at

$$\left| \int_u^1 \left(\frac{1}{\sqrt{x(x-\beta)}} - \frac{1}{x} \right) dx \right| \leq 2 \ln \left(\frac{1 + \sqrt{1+|\beta|}}{1 + \sqrt{1-|\beta|}} \right) \leq 2 \ln(1 + \sqrt{2})$$

Finally, we have:

$$|h_1(u)| \leq \frac{2 \ln(1 + \sqrt{2})}{\sqrt{1-u_0}}.$$

In a second step, we analyze the h_2 - function. We have:

$$|h_2(u)| \leq \int_u^1 \frac{dx}{x} \left| \frac{1 - bx - \sqrt{(1-x)(1-x/\alpha)}}{\sqrt{(1-x)(1-x/\alpha)}} \right| \leq \int_u^1 \frac{dx}{x} \frac{1 - \sqrt{1-x}}{\sqrt{1-x}}.$$

The upper bound of h_2 can be exactly integrated:

$$|h_2(u)| \leq \left| [-2 \ln(1 + \sqrt{1-x})]_u^1 \right| \leq 2 \ln(2)$$

We finally get:

$$F_{a,b,c}(u) = \frac{h_{a,b,c}(u)}{\sqrt{ab}} - \frac{\ln u}{\sqrt{ab}},$$

where $h_{a,b,c} = h_1 + h_2$ is a bounded function with

$$|h_{a,b,c}(u)| \leq \frac{2 \ln(1 + \sqrt{2})}{\sqrt{1-u_0}} + 2 \ln(2).$$

which is the bound used in the main text. Note that the bound on $h_{a,b,c}$ does not depend on a , b and c but only on a fixed parameter u_0 which can be chosen at will in $]0, 1[$. We denote by M the function defined by $M(u_0) = \frac{2 \ln(1 + \sqrt{2})}{\sqrt{1-u_0}} + 2 \ln(2)$ for $u_0 \in]0, 1[$. The derivative $h'_{a,b,c}$ of $h_{a,b,c}$ is given by the corresponding integrands of h_1 and h_2 , leading to:

$$h'_{a,b,c}(u) = \frac{1}{u} - \frac{1}{\sqrt{u(u+c/b)}} \frac{1-bu}{\sqrt{(1-u)(1+ub/a)}}.$$

Proposition 1. *For all $u_0 \in]0, 1[$, for all c such that*

$$0 \leq |c| < be^{-2\pi\sqrt{ab}-M(u_0)}, \quad (12)$$

for ab large enough, the equation

$$F_{a,b,c}(u) = 2\pi \quad (13)$$

has a unique solution $u = u_S(a, b, c)$ in $] \frac{c}{b}, u_0[$, which verifies:

$$\left| \frac{c}{b} \right| < u_S < e^{-2\pi\sqrt{ab}+M(u_0)}$$

and, in particular,

$$\lim_{ab \rightarrow +\infty} u_S(a, b, c) = 0.$$

Proof. Equation (13) becomes:

$$\frac{1}{\sqrt{ab}} h_{a,b,c}(u) - \frac{1}{\sqrt{ab}} \ln u = 2\pi \quad (14)$$

Equation (14) can be expressed in terms of a fixed point problem $u = f(u)$, with

$$f(u) = e^{-2\pi\sqrt{ab}+h_{a,b,c}(u)}.$$

We arrive at:

$$e^{-2\pi\sqrt{ab}-M(u_0)} < f(u) < e^{-2\pi\sqrt{ab}+M(u_0)}. \quad (15)$$

We show by continuity the existence of a solution to the fixed point problem if $f(|\beta|) > |\beta|$ and $f(u_0) < u_0$. The first condition is given by Eq. (12) while the second inequality is trivially verified from Eq. (15), for ab large enough. The uniqueness of the solution is verified if the function $g : u \mapsto f(u) - u$ is strictly decreasing. We show this statement for $c \leq 0$, while for $c > 0$, we prove that g is increasing on $[[\beta], u_m[$, it reaches its maximum in $u = u_m$ and is strictly decreasing on $]u_m, u_0[$.

Let us first consider the case $c \leq 0$. The function $h'_{a,b,c}$ can be bounded for $u \in]|\beta|, u_0[$ by:

$$h'_{a,b,c}(u) \leq \frac{1}{u} \left(1 - \frac{1 - bu}{\sqrt{(1-u)(1+ub/a)}} \right) \leq t(u)$$

where

$$t(u) = \frac{1}{u} (1 - (1-u)^{-1/2}).$$

Since $\lim_{u \rightarrow 0} t(u) = -\frac{1}{2}$ and t is a strictly decreasing function, we deduce that $h'(u) \leq -\frac{1}{2}$ for $u \in]|\beta|, u_0[$. g is therefore also strictly decreasing.

We then study the case $c > 0$. A zero u_m of g' fulfills:

$$h'_{a,b,c}(u_m) e^{h_{a,b,c}(u_m)} = e^{2\pi\sqrt{ab}},$$

then:

$$e^{2\pi\sqrt{ab}-M(u_0)} < h'_{a,b,c}(u_m) < e^{2\pi\sqrt{ab}+M(u_0)} \quad (16)$$

For ab large enough, Eq. (16) shows that u_m belongs to a small neighborhood of $u = |c/b|$ when $|c/b| \ll 1$. Moreover, the function $h'_{a,b,c}$ can be bounded by:

$$h'_{a,b,c}(u) \leq r(u),$$

where $r(u) = \frac{1}{u} - \frac{1}{\sqrt{u(u+|c/b|)}\sqrt{1-u}}$. We have:

$$r(u) \leq 0 \Leftrightarrow u^2 + |c/b|u - |c/b| > 0.$$

We obtain that $r(u) \leq 0$ and $h'_{a,b,c} \leq 0$ if $u \geq \sqrt{|c/b|}$ when $|c/b| \rightarrow 0$. In the interval $[[c/b], \sqrt{|c/b|}]$, $h'_{a,b,c}$ is equivalent for $|c/b| \ll 1$ to:

$$h'_{a,b,c}(u) \simeq \frac{1}{u} - \frac{1}{\sqrt{u(u+|c/b|)}},$$

which is a strictly decreasing function tending to $+\infty$ when u and c goes to 0. We deduce that there exists a unique u_m such that $g'(u_m) = 0$. We finally obtain that $g(u_m) > 0$ and that $g'(u) < 0$ in $]u_m, u_0[$, which leads to the uniqueness of the solution u_S . \square

Using Proposition 1, we can deduce Theorem 1 of the main text.

Proof. The proof follows directly from Proposition 1 and the relation $\Delta\phi_{a,b,c}(\epsilon) = F_{a,b,c}(\sin^2 \epsilon)$, since the change of variables $u = \sin^2 \epsilon$ is a bijection from $[0, \pi/2]$ to $[0, 1]$. \square

Note that Proposition 1 and Theorem 1 can alternatively be proved using the fixed point theorem. For ab large enough, the condition (15) gives that $f :]|\beta|, u_0[\rightarrow]|\beta|, u_0[$. The above proof was used because it gives in addition an interval in which the respective fixed points u_S and ϵ_S of f and $f \circ \arcsin$ belong, showing thus the corresponding limits for u_S and ϵ_S , when $ab \rightarrow +\infty$. On the other hand, the fixed point theorem also shows the robustness of the phenomenon.

2.2 Analysis of the region $u < |\beta|$.

We consider now the function $F_{a,b,c}$ in the region $|u| < |\beta|$. We recall that this analysis only concerns the case with $c > 0$ and that the result of Eq. (9) of the main text does not hold.

Lemma 1. *There exists a holomorphic function k defined on*

$$\mathcal{D} = \{v \in \mathbb{C} : |v| < \sqrt{|\beta|}\}$$

such that

$$F_{a,b,c}(u) = k(\sqrt{u})$$

i.e. $F(v^2) = k(v)$.

Proof. Turning around the origin in u , we do not catch the cycle δ as in the TRE, but a non-closed path. Turning twice around $x = 0$, we catch a closed cycle $\tilde{\delta}$ winding twice around the branch point $x = 0$ only. Note that here $\int_{\tilde{\delta}} \omega = 0$. The result is equivalent to integrate $x \mapsto \frac{1}{\sqrt{x}}$ on a loop winding twice around zero. Let k be $k(v) = F_{a,b,c}(v^2)$. Then, we deduce that:

$$k(v e^{2\pi i}) = F_{a,b,c}(v^2 e^{4\pi i}) = F_{a,b,c}(v^2) + \int_{\tilde{\delta}} \omega = F_{a,b,c}(v^2) = k(v).$$

Moreover, $k(0) = \int_0^1 \omega < \infty$ is a complete elliptic integral. Hence, k has a removable singularity at the origin and extends to a holomorphic function on \mathcal{D} . \square

Equation $\Delta \phi_{a,b,c}(\epsilon) = F_{a,b,c}(\sin^2 \epsilon)$ becomes

$$h_{a,b,c}(\sin^2 \epsilon) = 2\pi,$$

where $h_{a,b,c}$ is a bounded and analytic function. Note that the nature of this equation, valid in the small region \mathcal{D} is completely different from Eq. (14).

3 Analysis of the Monster Flip

We study in this section the Monster Flip for a standard skate board. As in the main text, we introduce the function $\tilde{F}_{a,b,c} = \int_{\cos^2 \psi_i}^{\sin^2 \epsilon}$ and search for solutions of

$$\tilde{F}_{a,b,c}(u) = 2\pi, \quad 0 \leq u \leq 1, \quad (17)$$

in the rotating case or

$$\tilde{F}_{a,b,c}(u) = 2\pi, \quad |\beta| \leq u \leq 1, \quad (18)$$

for oscillating trajectories. Note that $\cos^2 \psi_i$ is equal to 0 or to $|\beta|$ in the rotating and oscillating cases, respectively. Following the study used in TRE, we consider the two regions $0 < u < |\beta|$ and $|\beta| < u < 1$. In the case $0 < u < |\beta|$, which only concerns rotating trajectories, it can be shown that:

$$\tilde{F}_{a,b,c}(u) = \tilde{h}_{a,b,c}(\sqrt{u}),$$

where $\tilde{h}_{a,b,c}$ is a holomorphic function vanishing at the origin. For the region $|\beta| < |u| < 1$, we get:

$$\tilde{F}_{a,b,c}(u) - \ln(u) \int_{\delta}^u \omega = \frac{1}{\sqrt{ab}} \tilde{h}_{a,b,c}(u),$$

where $\tilde{h}_{a,b,c}$ is a single-valued function.

We consider now the different integrals in the real domain. Starting from the equation $\Delta\phi_{a,b,c} = \tilde{F}_{a,b,c}(u)$, we deduce that

$$\tilde{F}_{a,b,c}(u) = e^{2\pi\sqrt{ab} + \tilde{h}_{a,b,c}(u)}. \quad (19)$$

Approximate expressions of the variation ϵ can be obtained as follows. When $u \ll 1$, we have:

$$\tilde{F}_{a,b,c}(u) = \frac{1}{b} \int_{\cos^2 \psi_i}^u \frac{1 - bx}{\sqrt{x(x - \beta)(1 - x)(x - \alpha)}} dx \simeq \frac{1}{\sqrt{ab}} \int_0^u \frac{dx}{\sqrt{x(x - \beta)}},$$

where we have replaced x by 0 except in the factor $\sqrt{x(x - \beta)}$. A standard integration leads to:

$$\tilde{F}_{a,b,c}(u) \simeq \frac{2}{\sqrt{ab}} \ln \left(\sqrt{1 + \frac{u}{|\beta|}} + \sqrt{\frac{u}{|\beta|}} \right)$$

The equation $\Delta\phi_{a,b,c} = 2\pi = \tilde{F}_{a,b,c}(u)$ can then be approximated as:

$$\sqrt{1 + \frac{u}{|\beta|}} + \sqrt{\frac{u}{|\beta|}} = e^{\pi\sqrt{ab}}.$$

In the case $0 < u < |\beta|$, we have $\sqrt{1 + \frac{u}{|\beta|}} + \sqrt{\frac{u}{|\beta|}} \leq 1 + \sqrt{2}$ and we recover the fact that the $\tilde{h}_{a,b,c}$ -function is bounded. This also gives a strong constraint on the parameters a and b :

$$ab \leq \frac{[\ln(1 + \sqrt{2})]^2}{\pi^2}$$

The bound on the product ab is of the order of 0.079 which means that this situation is not very interesting in practice since the rigid body has to be slightly asymmetric. The variation ϵ of MFE can be estimated as:

$$\epsilon \simeq \pi\sqrt{ac}. \quad (20)$$

In the region $u > |\beta|$, a simple formula can be derived in the limit $u/|\beta| \gg 1$. A first order Taylor expansion leads to:

$$\epsilon \simeq \frac{\sqrt{|\beta|}}{2} e^{\pi\sqrt{ab}}, \quad (21)$$

which allows to estimate the bounded function $\tilde{h}_{a,b,c}$. These different approximations will be illustrated numerically in Sec. 4.

4 Numerical results

The goal of this paragraph is to illustrate numerically the different results established in this work. Figure 7 gives a general overview of the twist $|\Delta\psi|$ of the head of the racket when the handle makes a 2π -rotation. The twist is plotted as a function of the initial conditions ψ_0 and $d\psi/d\phi|_0$. In addition, this numerical result shows that the TRE and the MFE are not limited to the symmetric configuration analyzed in this study. We observe that TRE can be achieved in a large area around the separatrix. MFE occurs only in a very small band around the separatrix, which shows the difficulty to realize the Monster flip.

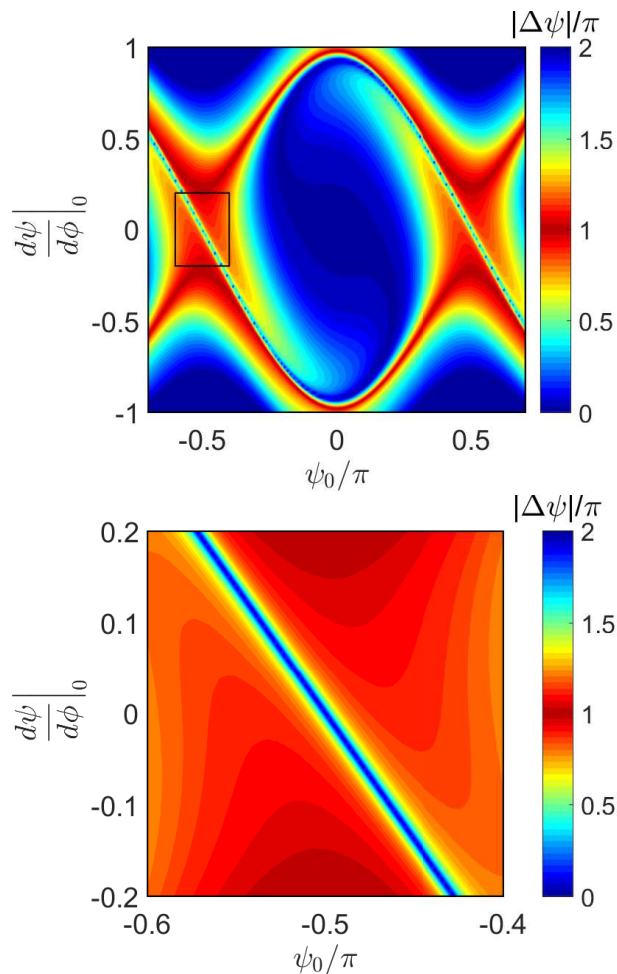


Figure 7: (Color online) (upper panel) Contour plot of the twist $|\Delta\psi|$, with $\Delta\phi = 2\pi$, as a function of the initial conditions ψ_0 and $d\psi/d\phi|_0$. (lower panel) Zoom of the upper panel corresponding to the black rectangle.

Figure 8 displays the evolution of ϵ in the TRE case. We observe that ϵ goes to zero when a increases. For the chosen value of the c parameter, it can be verified that $\epsilon > \epsilon_0$ for $a \leq 120$, with $\epsilon_0 = \arcsin[\sqrt{|c/b|}]$.

The behavior of ϵ in the MFE case is represented respectively in Fig. 9 and

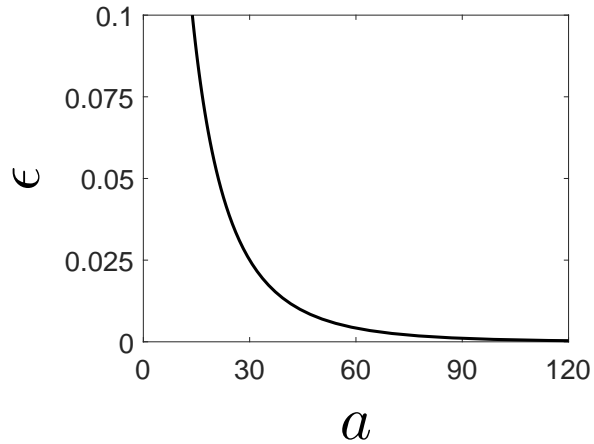


Figure 8: (Color online) Evolution of ϵ as a function of a in the TRE case. Parameters are set to $c = 10^{-9}$ and $b = 0.0629$, which leads to $\epsilon_0 = 1.26 \times 10^{-4}$.

10 in the region where $\epsilon < \epsilon_0$ and $\epsilon > \epsilon_0$. It can be seen that Eq. (20) and (21) give a very good estimate of ϵ . As could be expected, small values of ϵ are only obtained when c is sufficiently small. The parameters a and b have been chosen so that $ab \leq \frac{[\ln(1+\sqrt{2})]^2}{\pi^2}$ in the first situation.

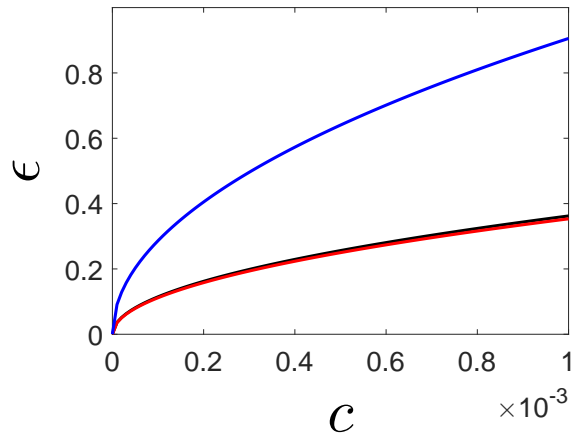


Figure 9: (Color online) Evolution of ϵ (black and red lines) and ϵ_0 (blue line) as a function of c in the MFE case. The black and red curves depict respectively the numerical solution and the approximate expression of ϵ given by Eq. (20). Parameters are set to $a = 12.65$ and $b = 0.0012$. Note that $ab < 0.079$.

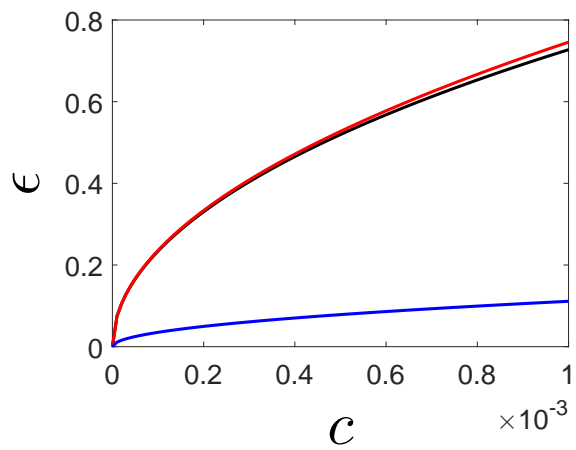


Figure 10: (Color online) Same as Fig. 9 but for the region $\epsilon > \epsilon_0$. The approximate expression of ϵ is given by Eq. (21). Parameters are set to $a = 8.82$ and $b = 0.0078$.